ARMY RESEARCH LABORATORY

U.S. Army Research Laboratory Directed Energy Internship Program 2013 Final Report

by Jeffrey O. White

ARL-TN-0589 January 2014

Approved for public release; distribution unlimited.

NOTICES

Disclaimers

The findings in this report are not to be construed as an official Department of the Army position unless so designated by other authorized documents.

Citation of manufacturer's or trade names does not constitute an official endorsement or approval of the use thereof.

Destroy this report when it is no longer needed. Do not return it to the originator.

Army Research Laboratory
Adelphi, MD 20783-1197

ARL-TN-0589 **January 2014**

U.S. Army Research Laboratory Directed Energy Internship Program 2013 Final Report

Jeffrey O. White
Sensors and Electron Devices Directorate, ARL

Approved for public release; distribution unlimited.

REPORT DOCUMENTATION PAGE

Form Approved
OMB No. 0704-0188

Public reporting burden for this collection of information is estimated to average 1 hour per response, including the time for reviewing instructions, searching existing data sources, gathering and maintaining the data needed, and completing and reviewing the collection information. Send comments regarding this burden estimate or any other aspect of this collection of information, including suggestions for reducing the burden, to Department of Defense, Washington Headquarters Services, Directorate for Information Operations and Reports (0704-0188), 1215 Jefferson Davis Highway, Suite 1204, Arlington, VA 22202-4302. Respondents should be aware that notwithstanding any other provision of law, no person shall be subject to any penalty for failing to comply with a collection of information if it does not display a currently valid OMB control number.
PLEASE DO NOT RETURN YOUR FORM TO THE ABOVE ADDRESS.

1. REPORT DATE *(DD-MM-YYYY)*	2. REPORT TYPE	3. DATES COVERED (From - To)
January 2014	Final	January 2013 to September 2013

4. TITLE AND SUBTITLE
U.S. Army Research Laboratory 2013 Directed Energy Internship Program Final Report

5a. CONTRACT NUMBER

5b. GRANT NUMBER

5c. PROGRAM ELEMENT NUMBER
622120

6. AUTHOR(S)
Jeffrey O. White

5d. PROJECT NUMBER

5e. TASK NUMBER

5f. WORK UNIT NUMBER

7. PERFORMING ORGANIZATION NAME(S) AND ADDRESS(ES)
U.S. Army Research Laboratory
RDRL-SEE-M
2800 Powder Mill Road
Adelphi, MD 20783-1197

8. PERFORMING ORGANIZATION REPORT NUMBER
ARL-TN-0589

9. SPONSORING/MONITORING AGENCY NAME(S) AND ADDRESS(ES)
High Energy Laser Joint Technology Office
801 University Blvd. SE, Suite 209, Albuquerque, NM 87106

Directed Energy Professional Society
7770 Jefferson Street NE, Suite 440, Albuquerque, New Mexico 87109

10. SPONSOR/MONITOR'S ACRONYM(S)
HEL-JTO, DEPS

11. SPONSOR/MONITOR'S REPORT NUMBER(S)

12. DISTRIBUTION/AVAILABILITY STATEMENT
Approved for public release; distribution unlimited.

13. SUPPLEMENTARY NOTES

14. ABSTRACT
This technical note is the final report for the 2013 Directed Energy Internship program at the U.S. Army Research Laboratory. Four interns were mentored by three Government employees. The projects included a fluorescence-based determination of quantum efficiency, the coupling efficiency between two fibers separated by an air gap, the fractal dimension of rare-earth energy levels, a power-scalable 2×2 opto-electronic combiner/router, and incoherent power combining of a megawatt-class high energy laser-diode system. The reports written by the interns are included as appendices.

15. SUBJECT TERMS
quantum efficiency, fiber coupling efficiency, fractal dimensions, power combining

16. SECURITY CLASSIFICATION OF:			17. LIMITATION OF ABSTRACT	18. NUMBER OF PAGES	19a. NAME OF RESPONSIBLE PERSON
a. REPORT	b. ABSTRACT	c. THIS PAGE			Jeffrey O. White
Unclassified	Unclassified	Unclassified	UU	40	19b. TELEPHONE NUMBER (*Include area code*) (301) 394-0069

Standard Form 298 (Rev. 8/98)
Prescribed by ANSI Std. Z39.18

Contents

List of Figures

List of Tables

INTENTIONALLY LEFT BLANK.

1. Introduction

The U.S. Army Research Laboratory (ARL) operated its 10th annual Directed Energy internship program in the summer of 2013, funded by the High Energy Lasers Joint Technology Office (HEL-JTO) and coordinated by the Directed Energy Professional Society (DEPS). This report summarizes the activities including recruitment, selection among applicants, and research areas pursued. Three of the four technical reports written by the participants are included as appendices; the fourth was submitted separately.

2. Recruitment of Participants

Applicants to the summer program were recruited using several methods. A Web page describing the program and our team's research topics were posted on ARL's Internet site and linked from the DEPS site. We also published a free ad in the *Physics Today* online classifieds, and asked the physics and electronic engineering (EE) departments at the University of Maryland (College Park and Baltimore County) and the University of Illinois to post advertisements or circulate via e-mail to their students. More than 50 students applied; one-third had credentials of sufficient quality and relevance to warrant serious consideration.

3. Selection of Participants

Twelve applicants were asked to furnish unofficial transcripts and two letters of recommendation; eight students furnished all of the required material. Summer internships were offered to five students; four accepted.

Linda Allee was a sophomore at the University of Arizona with a four-year scholarship, studying optical science and engineering and math. She was a good fit for Jeff White's projects on calculating fiber-to-fiber coupling efficiency, and fractal dimension of rare-earth energy levels (see appendix A).

Jason Chen was a freshman studying materials science at the University of Maryland. During the summer of 2012 he worked with Jun Zhang on design and engineering considerations for incoherent power combining of a megawatt-class high energy laser-diode system. He was the best candidate to work with Jun this summer on a study of using a high energy laser to remotely power an unmanned aerial vehicle (see appendix B).

Scott Melis was a junior at Loyola, Maryland University, working on a degree in physics. He was a good fit for Larry Merkle's project on a fluorescence-based determination of quantum efficiency.

Waylin Wing had just graduated from Central Michigan University with a degree in electrical engineering. In September 2013 he began graduate studies at the University of Alabama, Huntsville. He had worked with fiber ring lasers during an internship at the Center for Research and Education in Optics and Lasers (CREOL), so was a good fit for Jeff White's project on building an all-electronic optical switch with two fiber inputs and two fiber outputs (see appendix C).

4. Reporting of Student Research

All students submitted summaries of their research to the ARL student colloquium program. Jason Chen participated in the Sensors and Electron Devices Directorate student intern poster session at summer's end. The other students had already returned to school. Final reports were written by all four students. The full text of three reports is included in the appendices. The fourth has been published separately as ARL-CR-0726[1]

The primary reporting to the wider community has been the papers given at the Directed Energy Education Workshop. Linda Allee and Waylin Wing have prepared talks and posters to present at the 16th Annual Directed Energy Symposium, 10–14 March 2014.

5. Conclusion

We were pleased with the quality of all four of the DE interns this year. Even the students who were here for the first time more than repaid our investment in time and were well worth the stipend provided by the HEL-JTO. We continue to believe in the importance of training the future Department of Defense workforce and believe that the Directed Energy internship program provides students with an excellent, much-needed, close to real-life learning opportunity. One student, Waylin Wing, is applying for a Graduate Directed Energy Fellowship in High Energy Lasers.

[1]Melis, S. *A Fluorescence-Based Determination of Quantum Efficiency*; ARL-CR-0726; U.S. Army Research Laboratory: Adelphi, MD, December 2013.

Appendix A. Fractal Dimension, Coupling Efficiency, and Characterizing the Brillouin Spectrum By Linda Chardee Allee

A-1 Abstract

Three projects were completed this summer: fractal dimensions of rare-earth ions, coupling efficiency for two butt-coupled fibers, and characterizing the Brillouin gain spectrum (BGS). For the first project, a Matlab program was written to find the Hausdorff dimension of the energy levels of various rare-earth ions by using the box counting method. For the second project, another Matlab program was written to model Fresnel diffraction and simulate butt-coupling between two fibers. The program then finds the coupling efficiency for both longitudinal and lateral displacements. For the third project, data was collected for the characterization of the BGS of a ytterbium (Yb)-doped fiber amplifier by mixing the backscattered light with the original laser light on a photodiode, and using an electrical spectrum analyzer (ESA) to measure the difference frequency.

A-2 Acknowledgments

I would like to acknowledge the mentorship of Dr. Jeffrey White, Dr. Eliot Petersen, Dr. Carl Mungan, and Zhi Yang. All funding was provided by the High Energy Laser Joint Technology Office (HEL-JTO) and the Directed Energy Professional Society (DEPS). All work was conducted in the High Energy Fiber Laser lab located in Adelphi Laboratory Center (ALC) within the U.S. Army Research Laboratory (ARL).

A-3 Fractal Dimension Project

A-3.1 Introduction and Background

The energy levels of various rare-earth ions displays a pattern very similar to fractals (*1*), specifically, the Cantor set (figure A-1). A fractal is a self-similar pattern meaning the whole pattern is very similar or exactly the same as a sub-portion of the pattern and repeats itself at all scales (*2*). The Cantor set is formed by repeating the above line and removing the central third of each repetition (*3*). The Cantor set, along with other fractals, often has a non-integer Hausdorff dimension, a property describing the amount of space taken up by the pattern (*4*). Here the Cantor set has a dimension of approximately 0.6309 (*3*).

Figure A-1. Cantor set fractal.

A-3.2 Experiment and Calculations

Using a Matlab program to implement the box counting method, the fractal dimension of rare-earth ions was estimated by choosing different grid spacings between the lowest and highest energy level and finding the number of spaces that contain at least one energy level. Equations A-1 and A-2 describe a process for finding the Hausdorff dimension d:

$$N(r) = \frac{1}{r^d} \tag{A-1}$$

$$\ln(N) = -d * \ln(r) \tag{A-2}$$

where N(r) is the number of energy level grid elements of length r that contain energy levels. If a small grid size (r) is chosen, N will be large, meaning more grid sizes will contain energy levels (figure A-2). These changes in r can also be seen as changes in temperature.

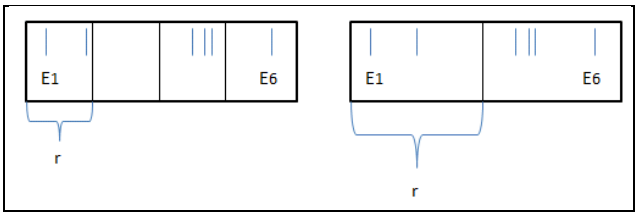

Figure A-2. Example of energy levels with different grid spaces (r).
On the left, N would be 3 and on the right N would be 2.

The program will ask the user to input energy levels and ask how the user wants to fit the data to find the dimension. For given energy levels, the program will find the difference for each combination of energy levels and use these spaces as grid sizes to test. The program can create a grid starting from either the lowest or highest energy level. A plot is generated of ln(N) vs. ln(r), where the negative of the slope is the approximate Hausdorff dimension of the energy levels. The results for erbium-doped yttrium aluminum garnet (Er:YAG) are shown in figure A-3.

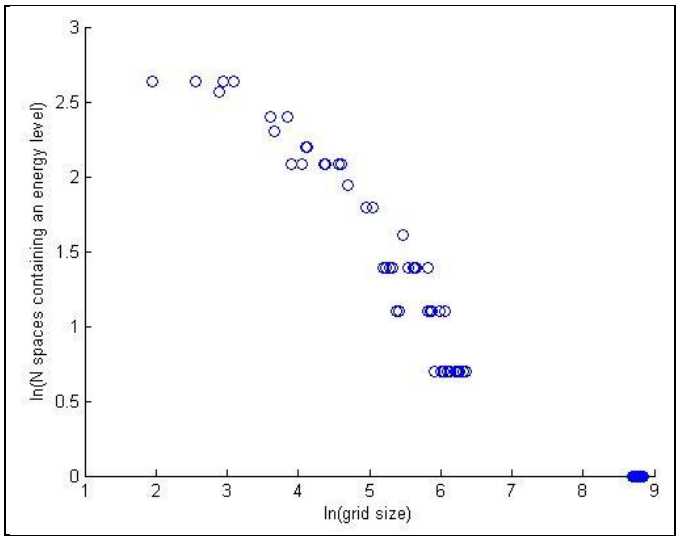

Figure A-3. Data points used to calculate the Hausdorff dimension of erbium-doped yttrium aluminum garnet (Er:YAG) at 77 K. The negative of the slope equals the approximate dimension.

The user can decide whether to fit the data on the left, right, or through the middle. The plots generated often have clusters of data in a horizontal line (figure A-4). This is because N often remains the same for small changes in r. Through the nature of the energy levels and their location, there are cases where with an increase in r, N also increases. This accounts for the slightly random nature of some of the points on the plot. The group of points at the end of the *x*-axis are a result of very large grid spacings where only one grid is needed (N=1) to contain the energy levels.

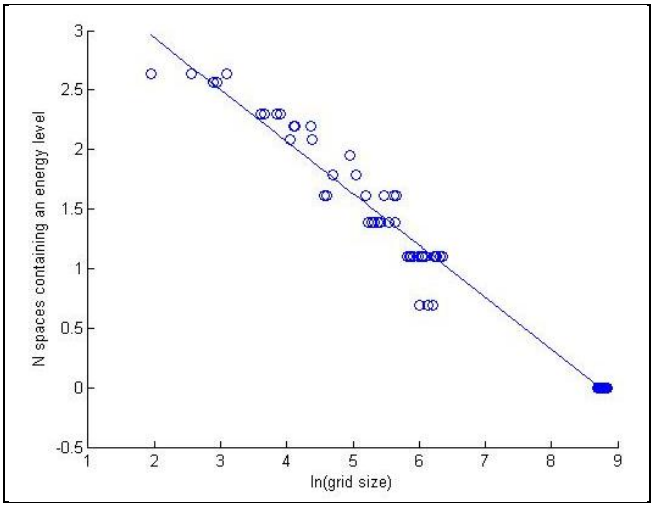

Figure A-4. Example of Er:YAG at 77 K with a fit along the middle of the points.

A-3.3 Results and Discussion

The Matlab program was run on Er, Yb, holmium (Ho), and neodymium (Nd) in YAG, scandia (Sc_2O_3), and yttria (Y_2O_3). The dimensions were non-integer and ranged between 0.370 and 0.528. In the case of Er:YAG, it was noted that with an increase in temperature, the dimension decreased. Table A-1 shows the dimension of various rare-earth ions for a certain temperature.

Table A-1. Dimension of various rare-earth ions for a certain temperature. Average dimension found by averaging different options for fitting the plot of ln(N) vs. ln(r).

Rare-Earth Compound	Temperature (K)	Dimension
Er:Sc_2O_3	77	0.478 ± 0.012
Er:YAG	77	0.463 ± 0.029
Er:YAG	300	0.441 ± 0.019
Er:Y_2O_3	77	0.461 ± 0.019
Ho:YAG	300	0.528 ± 0.033
Nd:YAG	300	0.503 ± 0.015
Yb:YAG	300	0.370 ± 0.017

A-3.4 Summary and Conclusions

A fractal dimension ranging between 0.370 and 0.528 was found for the energy level spectra of six rare-earth ions. Looking at Er:YAG, it can be seen that the dimension decreased with an increase in temperature. Fractal patterns occur throughout nature and understanding the properties of these patterns can facilitate our understanding of how certain rare earths behave both in lasers and in other occurrences.

A-4 Coupling Efficiency Project

A-4.1 Introduction and Background

Using an opto-mechanical 1x4 switch for butt-coupling two fibers separated by an air gap, it is important to know what losses to expect with different longitudinal and lateral misalignments between the fibers given fiber parameters (*5*). Here, the initial laser is propagating as the fundamental LP (0,1) mode in the first fiber. After exiting the fiber, the light undergoes diffraction and enters into the second fiber. For a longitudinal displacement of zero meters, with the fibers fused together, 100% of the light from the first fiber is coupled into the fundamental mode of the second where none of the other modes are excited. However, with any physical separation, diffraction between the fibers causes some of the light to couple into higher order modes while Fresnel reflections at each surface occurs, which causes some light to be lost. Matlab was used to find the coupling efficiency for various misalignments of the two fiber ends.

A-4.2 Experiment and Calculations

A Matlab program was written to find the overall coupling efficiency between two fibers with various longitudinal and lateral displacements. The wavelength of light propagating in the fiber was 1064 nm, the numerical aperture (NA) was 0.06, and the index of the core was 1.45 while

the index of the cladding was 1.4488. The diameter of the core was 25 microns while the diameter of the cladding was 400 microns. For the given parameters of the fiber being used, it was calculated that a total of four linearly polarized (LP) modes are capable of propagating in the fiber (figure A-5). The fundamental $LP_{0,1}$ mode was defined in the first fiber and propagated a certain distance using the Rayleigh-Sommerfeld diffraction integral while the higher order modes were defined in the second fiber. An overlap integral was then performed with the propagated fundamental mode and the higher order modes in the second fiber to find how much light is coupled into each of the four possible modes to find the corresponding coupling efficiency. The coupling efficiencies for each of the four modes are then added to find the total coupling efficiency.

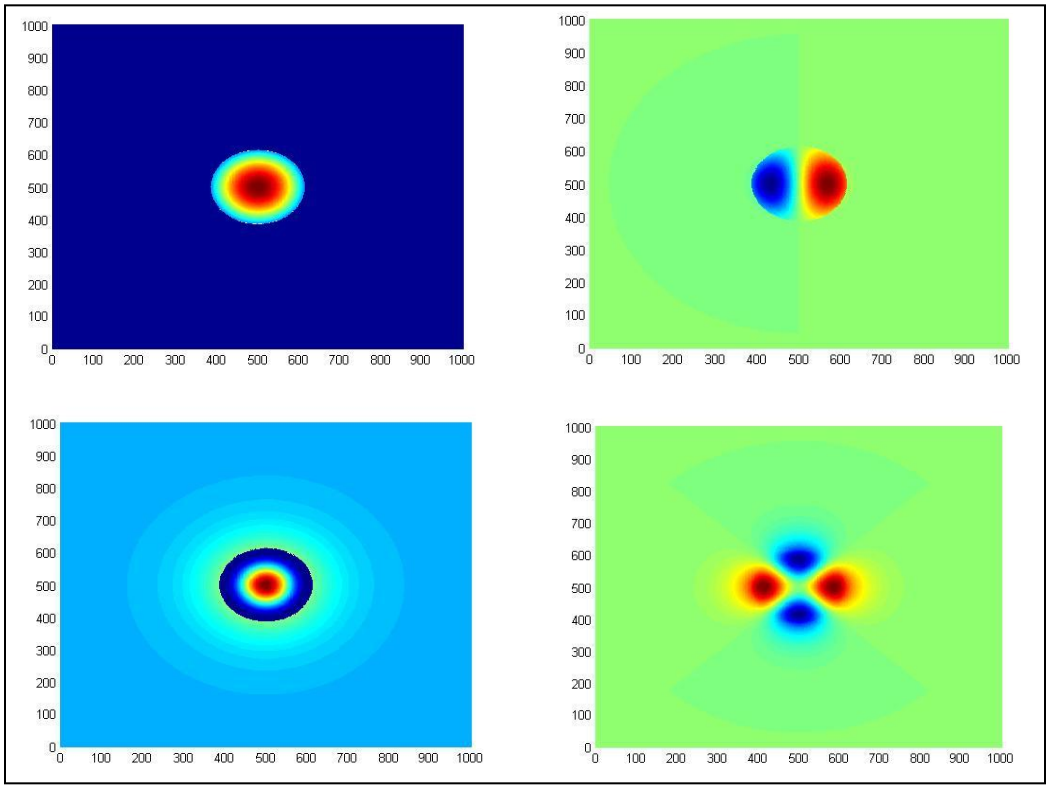

Figure A-5. The four LP modes capable of propagating through the fiber. From top left clockwise, (0,1), (1,1), (0,2), and (2,1).

The Rayleigh-Sommerfeld diffraction integral (*7*) is

$$E(x,y,z) = \frac{z}{i\lambda}\int_{-\infty}^{+\infty}\int E(x',y',0)\frac{e^{ikr}}{r^2}dx'\,dy' \qquad \text{(A-3)}$$

where x, y refer to the image plane (second fiber), while x' and y' refer to the source plane (first fiber). λ is the wavelength, z is the longitudinal distance between the two fibers, and k is the wavenumber given by

$$k = \frac{2\pi}{\lambda} \tag{A-4}$$

r is defined as

$$r = \sqrt{(x - x')^2 + (y - y')^2 + z^2} \tag{A-5}$$

and E(x',y',0) is the electric field for the core and cladding given by equations A-6 and A-7, respectively (*8*).

$$E = AJ_l(hr)e^{il\phi} \tag{A-6}$$

$$E = BK_l(qr)e^{il\phi} \tag{A-7}$$

Here, l is the azimuthal quantum number, Φ is the phase, A and B are constants, J_l is the Bessel function of the first kind, K_l is the modified Bessel function of the second kind, and h and q are given by equations A-8 and A-9, respectively (*8*).

$$h = \sqrt{\left(\frac{2\pi n_1}{\lambda}\right) - \beta^2} \tag{A-8}$$

$$q = \sqrt{\beta^2 - \left(\frac{2\pi n_2}{\lambda}\right)^2} \tag{A-9}$$

Note that n_1 is the index of the core, n_2 is the index of the cladding, and β is the propagation constant.

The overlap integral for coupling efficiency (*9*) is

$$\eta = \frac{\left|\int E_1^* E_2 dA\right|^2}{\int |E_1|^2 dA \int |E_2|^2 dA} \tag{A-10}$$

where η is the coupling efficiency, E_1 is the mode in the second fiber and E_2 is the diffracted fundamental mode from the source fiber.

A-4.3 Results and Discussion

Running the Matlab simulation for coupling efficiency, it was found that the maximum coupling efficiency for two butt-coupled fibers was approximately 93% due to Fresnel reflection losses. Total coupling efficiency dropped down to 50% for a fiber separation of approximately 400 microns, as seen in figure A-6. In figure A-7, it can be seen that almost all of the guided light was coupled into the fundamental mode of the fiber with only a small amount being coupled into the higher order modes. After the fundamental mode, the highest coupling

efficiency was approximately 5% into the (0,2) mode. For small longitudinal distances, the coupling efficiency decreased rapidly with lateral displacements while for larger longitudinal distances, the coupling efficiency decreased more slowly with the same lateral displacements shown in figure A-8.

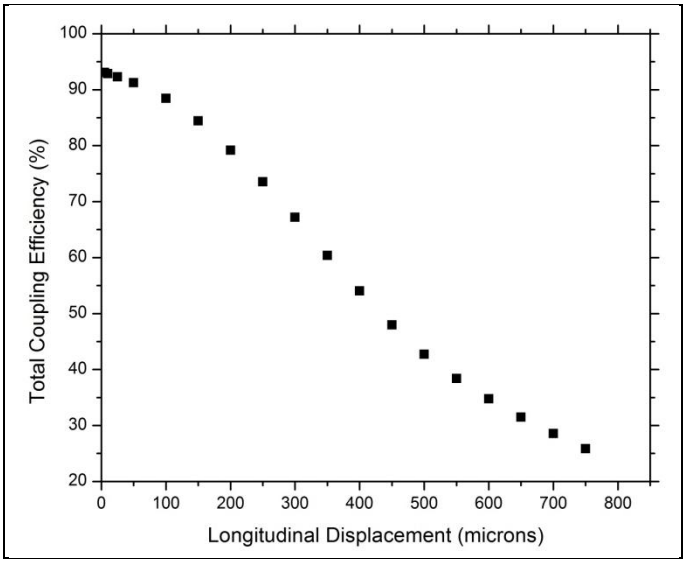

Figure A-6. Total coupling efficiency vs. longitudinal displacement.

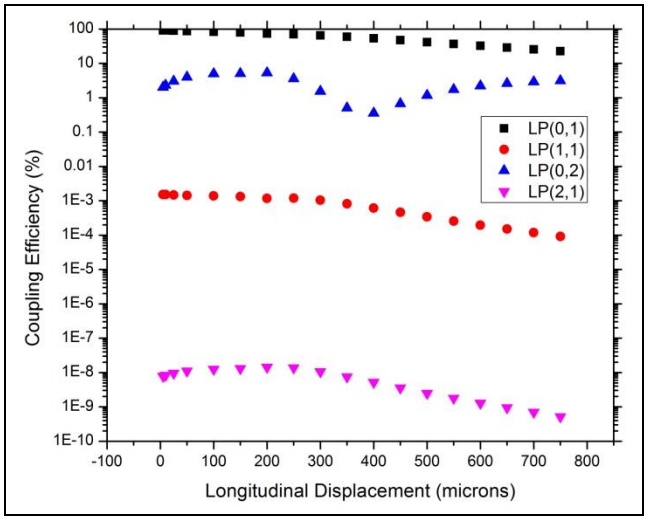

Figure A-7. Coupling efficiency for each of the possible modes vs. longitudinal displacement.

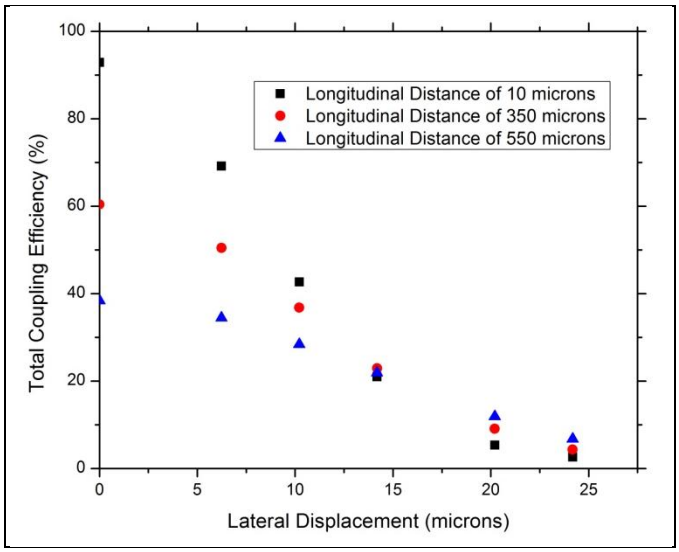

Figure A-8. Coupling efficiency vs. lateral displacement for different longitudinal displacements.

A-4.4 Summary and Conclusions

To test these simulation results, experiments can be performed to find maximum feasible coupling efficiency for given alignment and space constraints. Butt-coupling can be tested along with different lens combinations including both spherical and aspherical lenses. With no significant loss of energy, coherent combining of multiple high power fiber lasers becomes possible through the use of a 1x4 opto-mechanical switch.

A-5 Brillouin Spectrum Project

A-5.1 Introduction and Background

Brillouin scattering, the scattering of light from acoustic phonons, is a spontaneous linear process that can become stimulated and nonlinear at high powers within optical fiber. In the spontaneous regime, when the optical power is low, scattering occurs off thermal acoustic phonons, which cause index perturbations that scatter the incident light. In the stimulated regime, with high optical power, the backscattered wave (Stokes wave) can become very large This occurs as the forward and backward propagating waves interfere and through electrostriction, an acoustic wave is generated that reinforces the scattering process. This acoustic wave will further amplify the Stokes wave, which results in an exponential increase of the Brillouin scattering referred to as SBS (*6*).

A-5.2 Experiment and Calculations

The Brillouin spectrum of a Yb-doped fiber amplifier was characterized by mixing the back scattered light with the original laser on a photodiode and observing the resultant beat frequency on an ESA. Data were taken for the FWHM of the Brillouin gain spectrum (BGS) for various output powers. Figure A-9 shows the experimental setup.

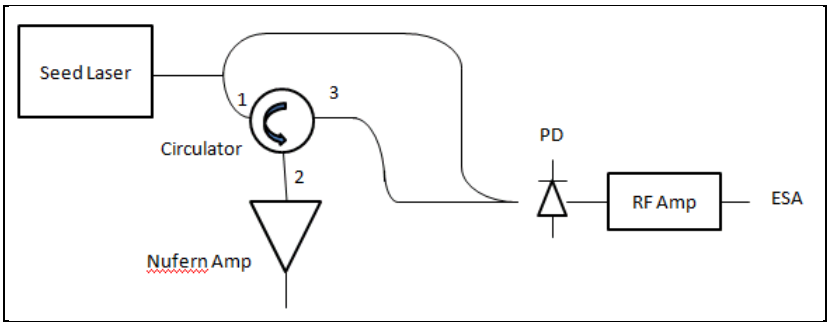

Figure A-9. Experimental setup for characterizing the Brillouin spectrum using a 50/50 splitter to mix the original laser and the backscattered light from the circulator on the photodiode.

A-5.3 Results and Discussion

The Brillouin frequency shift was 16.2 GHz. In the stimulated Brillouin region, the Brillouin gain bandwidth narrows to approximately 22 MHz for an amplifier output power of 3.47 W. The full width at half maximum (FWHM) increased with decreasing output power until the spontaneous region was reached for powers less than 1 W, where the width remained constant at approximately 55 MHz, which corresponds to the spontaneous Brillouin linewidth (figure A-10).

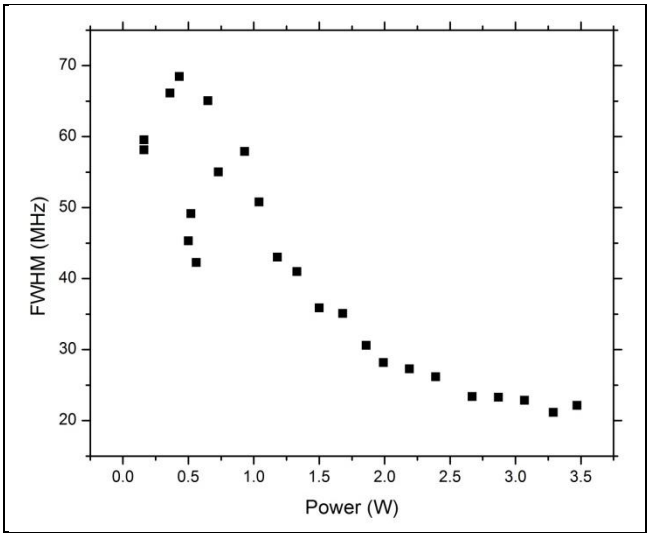

Figure A-10. Plot of Brillouin FWHM vs. power.

For low powers, the signal-to-noise ratio decreases and multiple peaks became evident (figure A-11). This makes fitting the peaks in the spontaneous region more difficult resulting in a large range of values for the spontaneous Brillouin linewidth. As output power increases, the peak on the left remained the same intensity, while the peak in the middle and on the right both increased with the peak on the right increasing much faster than the peak in the middle. As a result, for high powers, the peak on the right dominates the stagnant peak on the left and the slowly increasing peak in the middle (figure A-12).

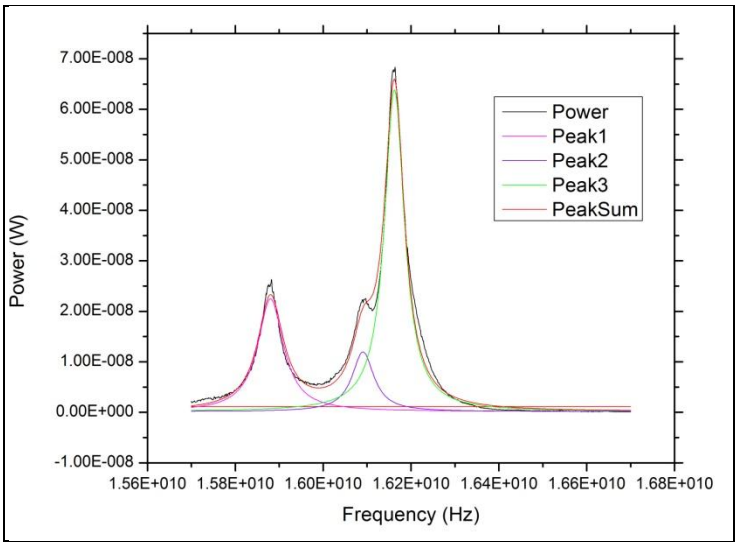

Figure A-11. BGS plot at low output power, 0.73 W, the right peak has FWHM = 55 MHz using a Voigt fit.

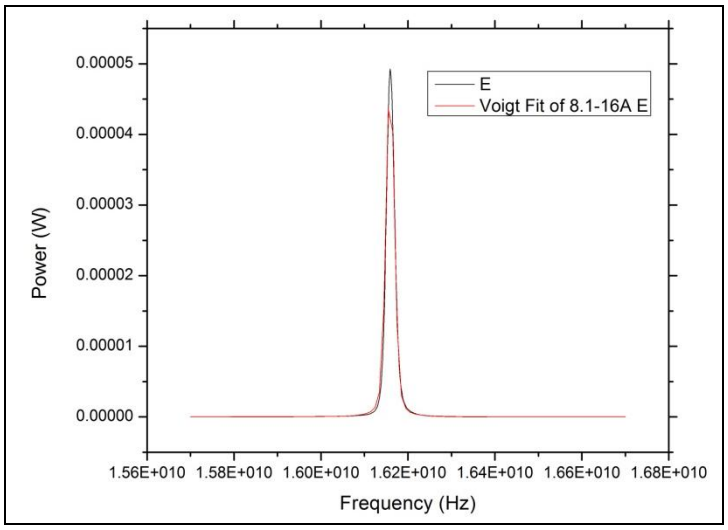

Figure A-12. BGS plot for high power, 3.47 W, FWHM = 22 MHz using a Voigt fit.

A-5.4 Summary and Conclusions

Further experimentation can be done to find the source of the peaks in the middle and on the left in the low power BGS graph. Using the characteristics from the BGS, the stimulated Brillouin scattering threshold (SBST) can be found for this fiber amplifier. Threshold occurs when the Stokes wave reaches a certain percentage of the output light.

A-6 References

1. Cummings, A.; O'Sullivan, G.; Hanan, W. G.; Heffernan, D. M. Multifractal Analysis of Selected Rare-Earth Elements. *J. Phys. B: At. Mol. Opt. Phys.* **2001**, *34*, 2547.
2. WolframMathWorld, "Self-Similarity," http://mathworld.wolfram.com/Self-Similarity.html (accessed 2013).
3. ORACLE ThinkQuest Education Foundation, "Cantor Set," http://library.thinkquest.org/26242/full/fm/fm3.html (accessed 2013).
4. WolframMathWorld, "Hausdorff Dimension," http://mathworld.wolfram.com/HausdorffDimension.html (access 2013).
5. Bisbee, D. L. Measurements of Loss Due to Offsets and End Separations of Optical Fibers. *The Bell System Technical Journal* **1971**, *50* (10), 3159–3168.
6. Kobyakov, A.; Saur, M.; Chowhury, D. Stimulated Brillouin Scattering in Optical Fibers. *Advances in Optics and Photonics* **2010**, *2* (1), 1–59.
7. Volez, David. *Computational Fourier Optics A MATLAB Tutorial*; Bellingham: SPIE Press, 2011.
8. Yariv, A. *Optical Electronics 3rd Edition*, Chapter 3; CBS College Publishing, New York, 1985.
9. RP Photonics Encyclopedia, "Mode Matching," http://www.rp-photonics.com/mode_matching.html (accessed 2013).

INTENTIONALLY LEFT BLANK.

Appendix B. In-Flight Charging of a UAV Using High Energy Laser by Jason Chen

B-1 Abstract

In-flight refueling is a game-changing technology to the military. Development of in-flight charging technology of battery-powered unmanned aerial vehicles (UAVs) is potentially important to the future Army capability. This study explores the potentials and engineering parameters of using a high energy laser as a power source to remotely power and charge an in-flight light-frame UAV. Power budget and power conversion efficiency from a ground laser to a UAV engine have been estimated and calculated. A high energy diode-based laser system, target tracking and laser beam delivery, and single band-gap photovoltaic (PV) panel have been individually studied for the application. Ground diode laser system with up to hundreds of kilowatts has been proposed for the application. In this study, we also proposed and planned to build a prototype of a flying radio-controlled (RC) helicopter remotely powered by a 40-W laser beam as a proof-of-concept demonstration.

B-2 Acknowledgments

I wish to acknowledge the mentorship of Jun Zhang

B-3 Student Bio

Jason Chen currently goes to school at the University of Maryland at College Park. He is an undergraduate freshman majoring in mechanical engineering and will graduate in 2016. Chen has done summer research at ARL in Adelphi, MD, for 3 years (2011–2013). His research includes the design and construction of a Hall measurement probe station, engineering and design considerations for incoherent power combining of megawatt-class high energy laser-diode laser system, and research in in-flight charge of UAVs using high energy laser.

B-4 Introduction/Background

UAVs are playing an increasingly important role in modern warfare. They are used for remote sensing, surveillance, reconnaissance, and even firing missiles. However, UAVs typically have limited flight duration due to fuel and battery constraints. Most UAVs can only fly for hours at a time before they have to land and refuel or recharge their battery. The necessity to constantly land UAVs is a big disadvantage to the military, because it takes away from mission time and landing UAVs is dangerous. A majority of destroyed UAVs are due to crashed landings, so extending flight time and being able to recharge in-flight would be a huge advantage. UAVs can cost millions of dollars and preserving them is very important.

Using a high energy laser to recharge a UAV in-flight would have the following benefits:

- Extend mission duration for UAVs
- Allow UAVs to fly longer distances
- Enable UAV surveillance over large areas through a network of charging stations.

Diode laser based high energy laser systems are able to provide and deliver hundreds of kilowatts of optical power to a small target in a few kilometers range. In addition, single band gap photovoltaic (PV) panel can efficiently convert optical power to electric power for the UAV power source. The high energy laser remote charging system can be very efficient with low cost.

B-5 Design

There are four key elements in the system: high energy diode laser, target tracking and laser beam delivery, single bandgap PV panel, and light-frame, battery-powered UAV.

B-5.1 High Energy Diode Laser

Up to a few hundred kilowatts combined laser output can be generated from efficient and low-cost diode lasers. The basic building blocks are ~100-W fiber-coupled laser modules. Output fibers are bundled together to achieve high energy/high brightness in 15-mm-diameter single aperture output. The fibers are bundled together in a honeycomb structure (figure B-1).

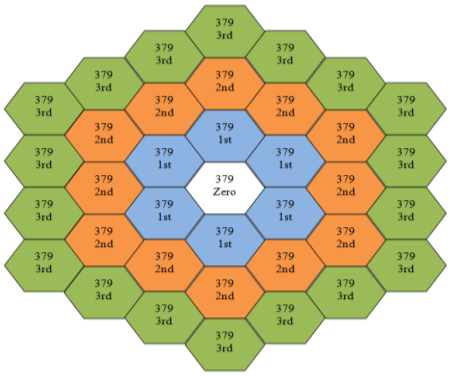

Figure B-1. Fibers are bundled in a honeycomb structure to generate kilowatts of power.

B-5.2 Target Tracking and Laser Beam Delivery

The beam director is designed for delivering high energy laser beam to the remote target. Tracking sensors on the beam director will locate the UAV and the PV panel, so the laser can be directed there.

Based on our previous work, laser power can be collimated with an ~1-m-diameter optical system. A laser beam size of ~1 m^2 is delivered to the remote target of up to 2 km range through the atmosphere.

The laser beam can only reach a certain distance, but creating a network of charging stations would allow unlimited flight and surveillance throughout the network.

B-5.3 Single Band Gap PV Panel

A PV panel consists of a connected assembly of PV cells that convert light energy to electrical energy. Because single bandgap PV cells are used, high conversion efficiency and high power density can be achieved for laser power conversion. Currently, up to 50% optical to electrical conversion efficiency can be achieved.

Single bandgap PV panels only accept light from a certain wavelength, while normal PV panels accept multiple wavelengths. The single bandgap PV panel will only accept light of the same wavelength as the laser. Because the laser is only a specific wavelength, the PV cells will absorb maximum optical energy to convert to electrical energy.

B-5.4 Light-Frame, Battery-Powered UAV

Light-frame UAVs are mostly designed for surveillance and reconnaissance. They have light payload and consume less power, which can be powered by high energy density batteries. Battery-powered UAVs could charge during flight using laser beaming, but in-flight refueling is not a feasible option currently.

B-6 Engineering Considerations

Initial electrical energy is generated from a power supply. The electrical energy is powered the fiber coupled and bundled diode lasers, which are collimated at the beam director. Tracking sensors on the beam director locate the UAV and the PV panel, and direct the collimated laser beam at the PV panel. The PV panel converts the optical energy back into electrical energy, which charges the battery. The battery is used to power the electrical engine of the UAV. Figure B-2 shows the system layout.

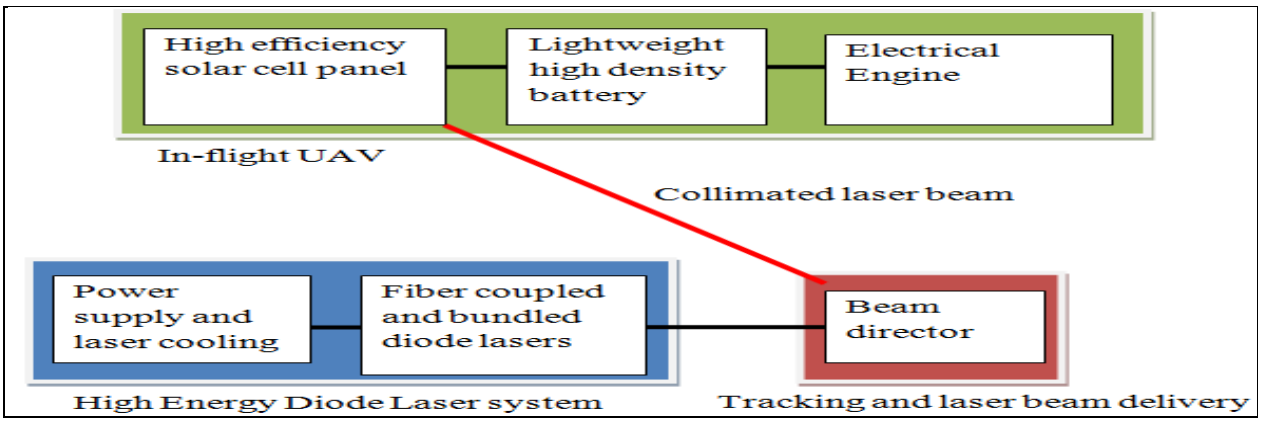

Figure B-2. System layout from laser to UAV.

B-6.1 System Efficiency

The efficiency of power transmitted from the laser to the UAV is affected by many different factors; air propagation, PV panel absorption, and electrical to optical conversion all negatively affect the efficiency. The total efficiency from the laser to the final electrical power is around 33% in this design. Improved PV panel optical to electrical energy conversion efficiency and diode laser electrical to optical conversion efficiency could great improve the overall efficiency for the system. Table B-1 shows the efficiency calculations.

Table B-1. Efficiency calculations.

Power Budget	Power			
	W	kW	kW	kW
Final electrical	13.01	0.33	6.50	32.51
PV panel optical to electrical	13.01	0.33	6.50	32.51
PV panel fill factor	26.01	0.65	13.01	65.03
Air loss	30.60	0.77	15.30	76.50
Telescope	34.00	0.85	17.00	85.00
Diode Optical	40.00	1.00	20.00	100.00
Electrical	80.00	2.00	40.00	200.00
Efficiency parameters			Efficiency	
Diode laser electrical to optical			0.50	
Telescope			0.85	
Air propagation			0.90	
PV panel fill factor			0.85	
PV panel optical to electrical			0.50	
Overall efficiency			0.33	

B-6.2 Prototype Demo

A 40-W diode powered RC helicopter demo prototype is designed and currently being built. The highlighted column in table B-1 represents basic power parameters. The RC helicopter will be directly powered by the laser beam rather than the battery. The helicopter will be placed in a fixed frame that only allows vertical motion. The purpose of this demo is to show that laser projection can be used as a viable power source. The RC helicopter is much lighter than any UAV and the laser is less powerful, but it illustrates the concept of in-flight charging using a laser. A more powerful laser could also power a heavier UAV.

B-7 Summary and Conclusions

Powering a UAV by projecting a laser is possible and can provide huge benefits to the military. It is a reliable wireless power source that would revolutionize military applications for the UAV by extending missions, flight time, and surveillance area. The UAV would not need to land as often and UAV crashes would occur less often as a result. UAVs have a large price tag and it is economically and militarily beneficial to employ in-flight charging of battery powered UAVs using a high energy laser.

B-8 References

Konkola, P. *Beam Directors for Optical Directed Energy: Beyond the Status Quo, Enabling Capabilities for the War Fighter.* 15th Annual Directed Energy Symposium, Albuquerque, NM, 2012.

Nugent, T. J.; Kare, J. T. *Laser Power for UAVs*. LaserMotive, 2010.

INTENTIONALLY LEFT BLANK.

Appendix C. Coherent Beam Combining Using an Electronically Controlled 2x2 Optical Switch by Waylin Wing

C-1 Abstract

An optical switch is designed to combine the output of two fiber amplifiers and direct the total power to either one of two delivery fibers. The switch operates by controlling the relative phase of the two beams incident upon the switch using a feedback loop consisting of photodiode sensors, a computer algorithm, a microprocessor, and acousto-optic frequency shifters. Possible applications, conclusions, and future work are discussed.

C-2 Acknowledgments

All work presented was conducted in the High Power Fiber Laser Lab within ARL at Adelphi, MD. Guidance from members of the High Power Fiber Laser Lab, specifically from Jeff White, Eliot Petersen, and Zhi Yang, is gratefully acknowledged. Work was made possible through funding by the High Energy Lasers Joint Technology Office (HEL-JTO) and the Directed Energy Professional Society (DEPS).

C-3 Literature Review

One technique to power-scale high-energy lasers past the fundamental limits for a single aperture source is to combine multiple laser beams together. The three main types of laser combining are side-by-side combining, coherent beam combining (CBC), and wavelength beam combining (WBC) (*1*). We employ CBC in our lab as the brightness scales as the number of emitting apertures squared.

CBC requires the laser beams being combined to be locked in phase and frequency, have a relative phase difference that results in maximum output power, and be made to produce uniform exit aperture illumination (*2*). A system designed to make use of CBC must address each requirement, otherwise significant degradation of the output power can be expected. The output power, expressed as radiance, of CBC and WBC systems is given by

$$B = \frac{CP}{\lambda^2 (M^2)^2} \tag{C-1}$$

where B is the radiance, C is a constant based on beam size and divergence angles, P is the power, λ is the wavelength, and M is the beam quality (*1*). The power scales as N number of elements increases, and the brightness (or intensity) scales as N^2 in the far field.

One of the limiting factors in the output power of each individual fiber laser amplifier is SBS. This builds up from scattering from thermal phonons having a wavelength of ~λ/2. When the

incident laser power is large enough the density fluctuations become stimulated and the scattering grows exponentially. One way to combat the effects of SBS is to use a linearly chirped seed to reduce the effective gain length for the Stokes wave (*3, 4*).

C-4 High Power Fiber Laser Combining at ARL

The High Power Fiber Laser Lab is using a linearly chirped 1064-nm seed laser to increase the (SBS) threshold of a Yb fiber amplifier, which will consequently increase the maximum output power. To combine two laser beams together, a configuration must be designed to accept these two beams and overlap them in space. An optical phase locked loop (OPLL) is used to maintain coherence between each channel and a reference beam. The relative phase difference between both channels is not fixed though, so another feedback loop must be used to maintain a fixed phase relationship between the two channels. Also, some sort of feedback mechanism is needed to prevent the relative phase between the beams from slipping. For these reasons, a 2x2 optical switch with electronic feedback has been designed.

C-5 2x2 Optical Switch

In order to create an optical switch that operates via interference, it's necessary to monitor and control the relative phase difference between the two input laser beams. To do this, the optical switch makes use of a feedback loop, which can request the OPLL to adjust the relative phase differences. There are two possible output locations; the output location containing the combined laser beam is determined by user input to a computer program. The block diagram of the phase control loop is shown in figure C-1.

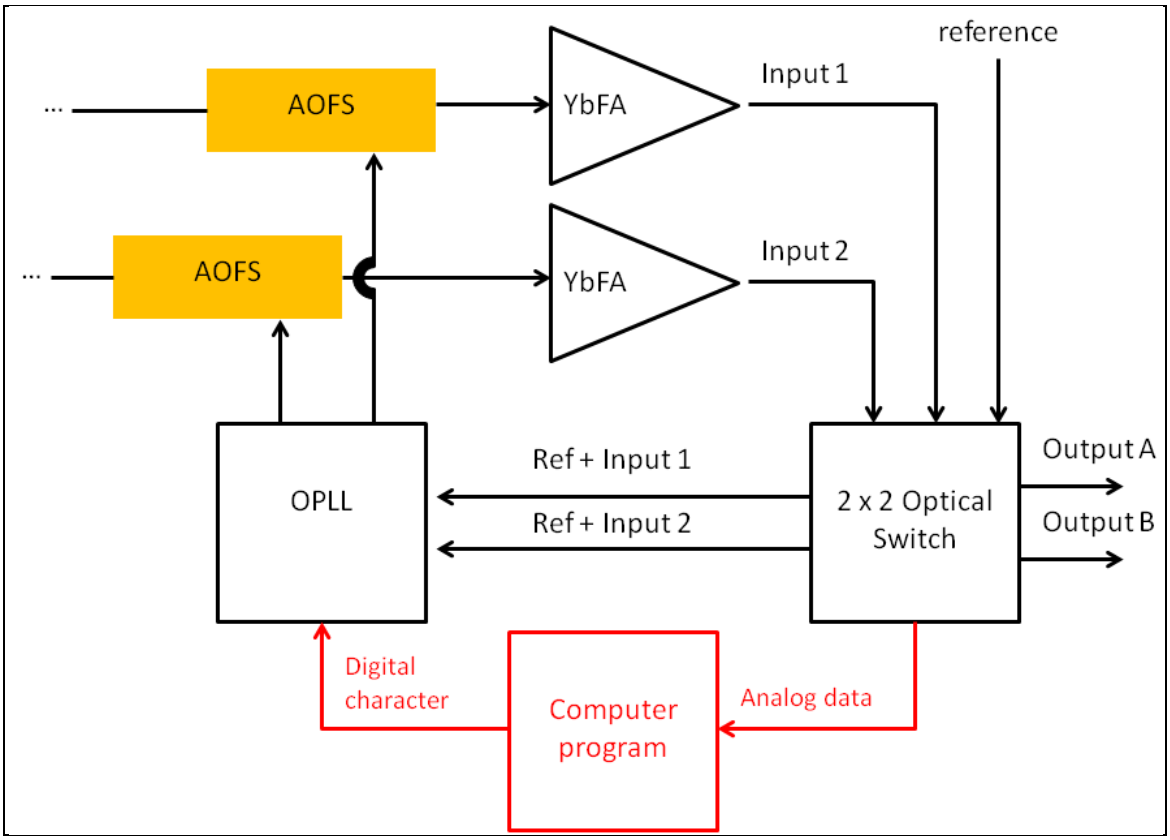

Figure C-1. The phase control loop used to monitor and control the relative phase difference between the two input laser beams. AOFS are the acousto-optic frequency shifters and YbFAs are the ytterbium fiber amplifiers. The computer feedback loop is shown in red.

C-5.1 Experimental Setup

A block diagram showing the inputs and outputs of the optical switch is shown in figure C-2. The experimental configuration of the switch is shown in figure C-3. The switch has two laser beam inputs, a reference beam input, two laser beam outputs, and four photodiodes that sample the output beams and monitor the interference between the reference and input beams. The reference beam is used to lock the phases of the two channels, i.e., to maintain a constant relative phase difference. Beam Sample A and Beam Sample B are used to determine if the phase between the two channels has the desired value. The optical switch contains simple optical components, such as mirrors, beam splitters, and wedges.

In order to increase the stability of the optical switch, custom aluminum mounts were made to support the four collimating and focusing objectives (figure C-4.)

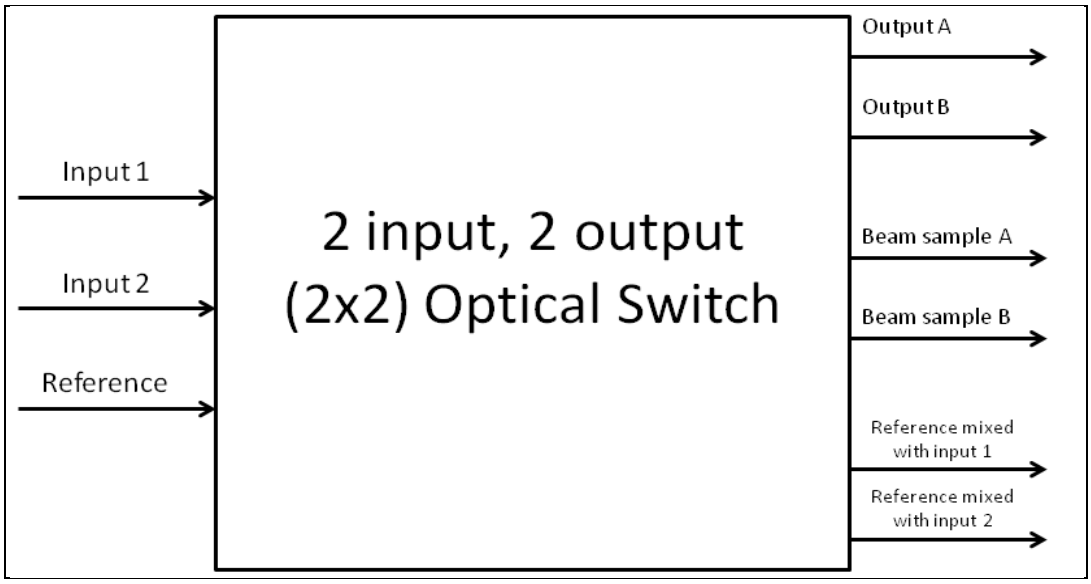

Figure C-2. Block diagram showing the input and output functions of the 2x2 optical switch.

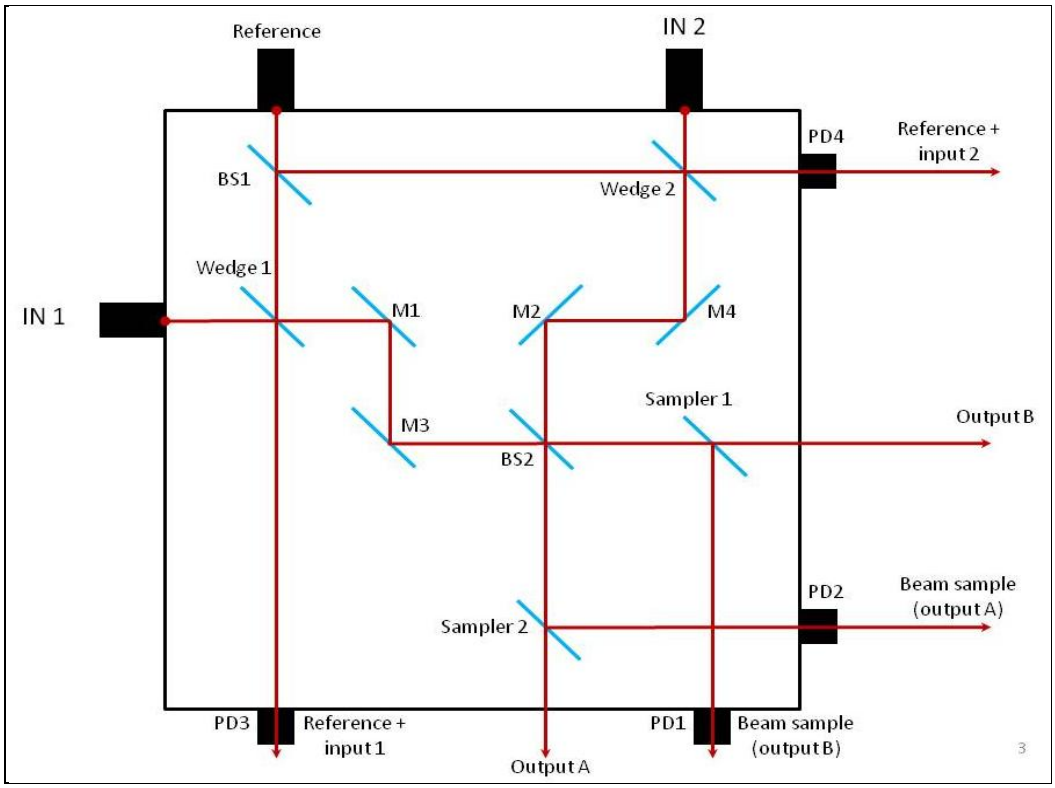

Figure C-3. The experimental setup of the 2x2 optical switch.

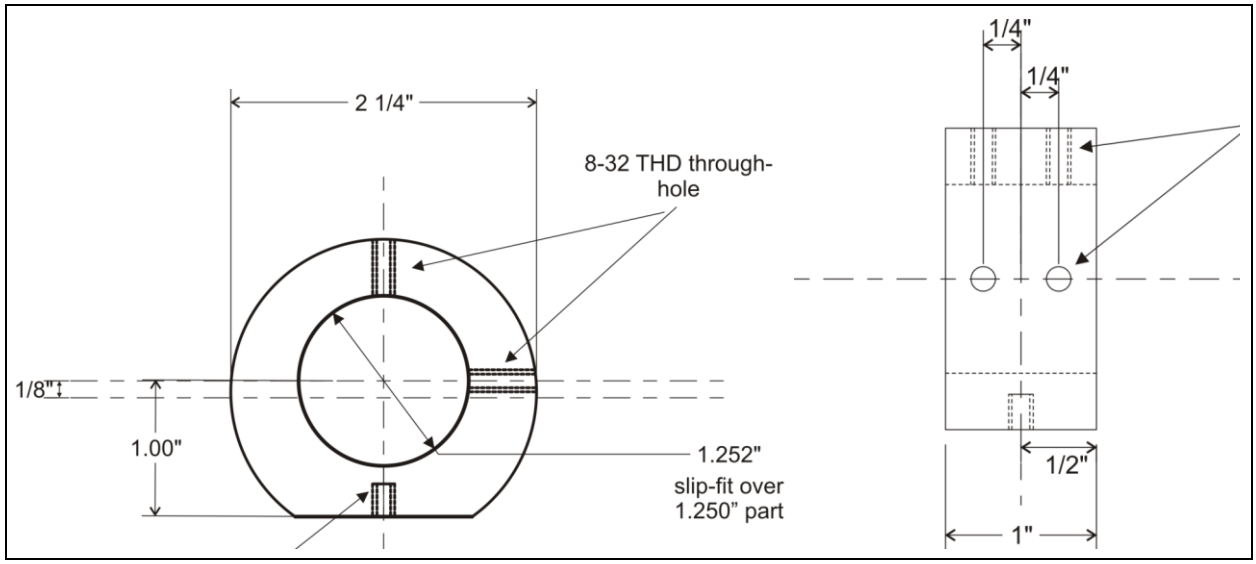

Figure C-4. The design for the custom collimating lens holder.

The components for the optical switch were placed on 1-in pedestals screwed to a 1 ft x1 ft aluminum breadboard. Alignment was achieved using the 1064-nm laser at low power. A photograph of the completed optical switch is shown in figure C-5.

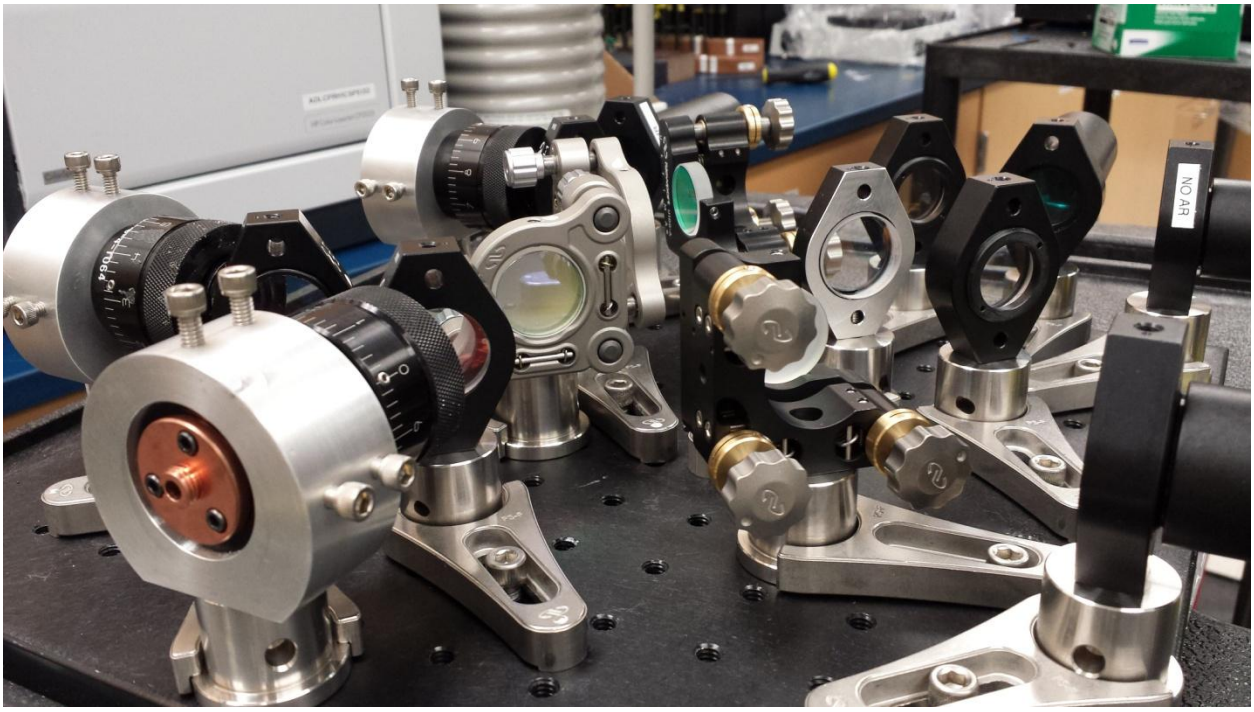

Figure C-5. A photograph of the optical switch.

C-5.2 Computer Control

The computer program used to control the phase was created using *LabWindows*. The program takes simple input from the user and is made to interface with the OPLL via a universal serial

bus (USB) connection. The user selects certain parameters (such as which communications port, which output will contain the beam; see figure C-6) and then initiates the program. Once initiated, the program starts to sample the voltage on the photodiode from Beam Sample A or B. The function of the program is to lock this voltage at either a maximum voltage or a minimum voltage that corresponds to the switch either being on or off at that output. The algorithm uses a dither in combination with the readings from the photodiode to decide whether or not the relative phase between the two input beams should be increased or decreased (figure C-7). After initiating the program, the phase is continually probed until a maximum is reached, at which point the dither and the input voltage will begin to oscillate. The OPLL is configured to receive ANSI C characters from the USB connection; therefore, an increase or decrease in the phase correlates to the computer sending certain characters to the OPLL. The computer feedback loop is shown in figure C-1, outlined in red.

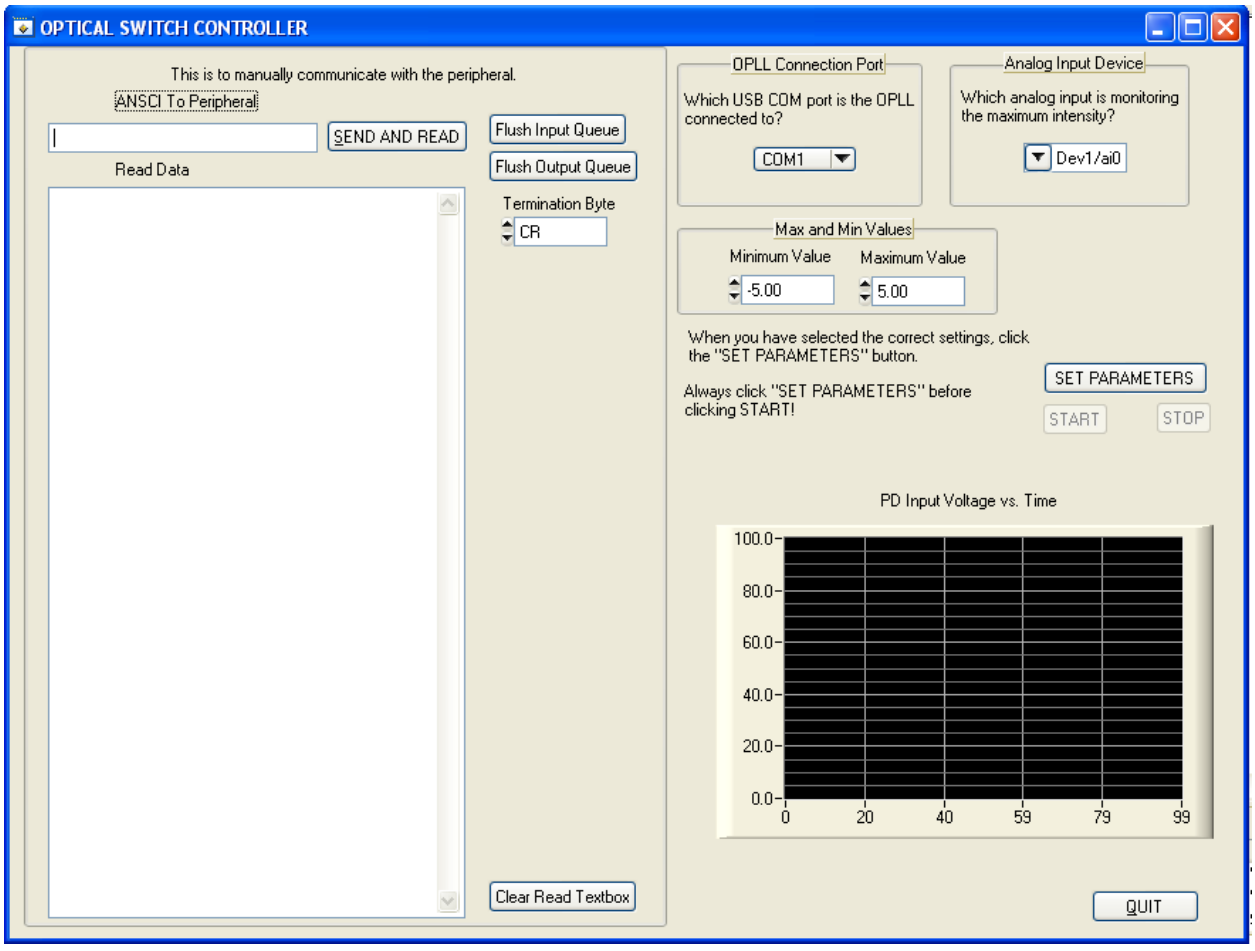

Figure C-6. The graphical user interface used by the computer program.

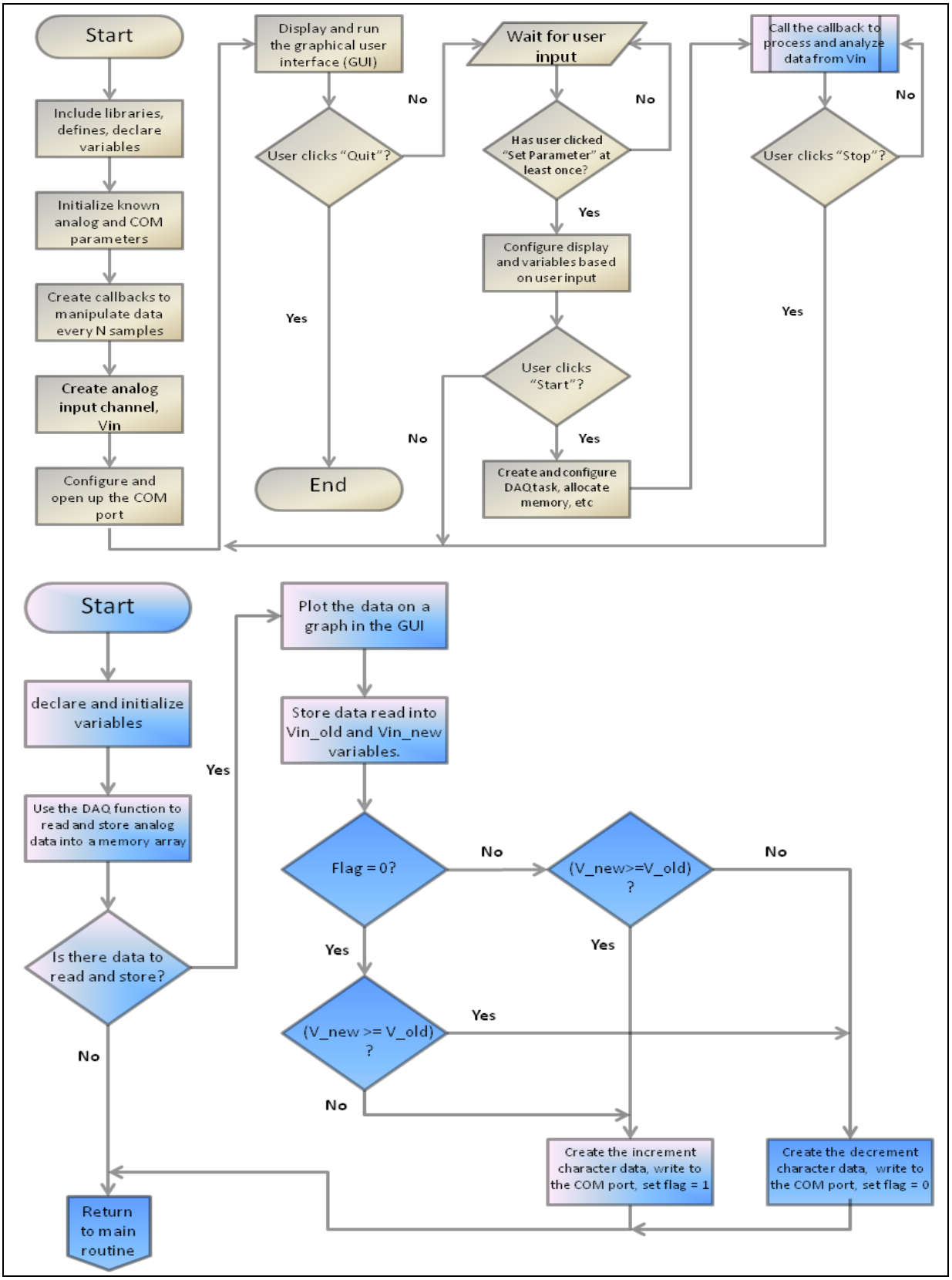

Figure C-7. (Top) The main computer program flowchart. (Bottom) The subroutine that contains the algorithm for adjusting the relative phase.

C-6 Applications

Laser combined, high-radiance sources have many uses in manufacturing, military, and commercial industries. CBC single-mode lasers are used to maintain beam quality over large distances. The defense industry will always benefit from the power-scaling that is inherent with laser beam combining. Higher radiances allow for a larger variety of threats to be eliminated.

The 2x2 optical switch has distinct advantages over single output high-energy lasers (HELs). An opto-electronic switch allows for very fast changing of outputs without having mechanical movement or limitations. The direct application of a 2x2 optical switch coupled with a HEL is for defense against large ballistic threats aimed at manned or unmanned vehicles. For instance, a high power optical switch could direct the combined power from two amplifiers to one of two delivery fibers leading to apertures that conform to the fuselage of a helicopter to prevent a surface-to-air attack.

C-7 Conclusions and Future Work

C-7.1 Conclusions

The optical switch was built and aligned. Custom mounts were designed for the collimating and focusing objectives. The LabWindows program was shown to work in the phase control loop and be compatible with the OPLL software that runs in parallel. Improvements need to be made to the experimental setup to make the switch more rugged. Improvements to the computer program need to be made to optimize the speed and stability.

C-7.2 Future Work

To improve the optical switch, a more stable way of mounting all the components could be explored. For example, the components could be mounted to a chassis machined from a single piece of aluminum. This would make all of the components interconnected, thus reducing the effect of disturbances on the system. Custom parts could make the switch smaller. A more compact switch would find wider applications. Enclosing it in a casing would keep dust and other contaminants from affecting the optics. At high energy, small contaminants on the components can cause catastrophic damage.

The computer program can be improved by streamlining the code and reducing the amount of unnecessary information. Also, the code could make use of arrays or other programming tools to reduce the amount of data used while the program is running. The graphical user interface of the program could be “cleaner” and contain more options.

In the future, the 2x2 optical switch concept could be extended to a switch with an arbitrary number of inputs and outputs. A 4x4 optical switch is pictured in figures C-8 and C-9. Notice that this switch is somewhat monolithic and uses the same concepts from the 2 x 2 switch.

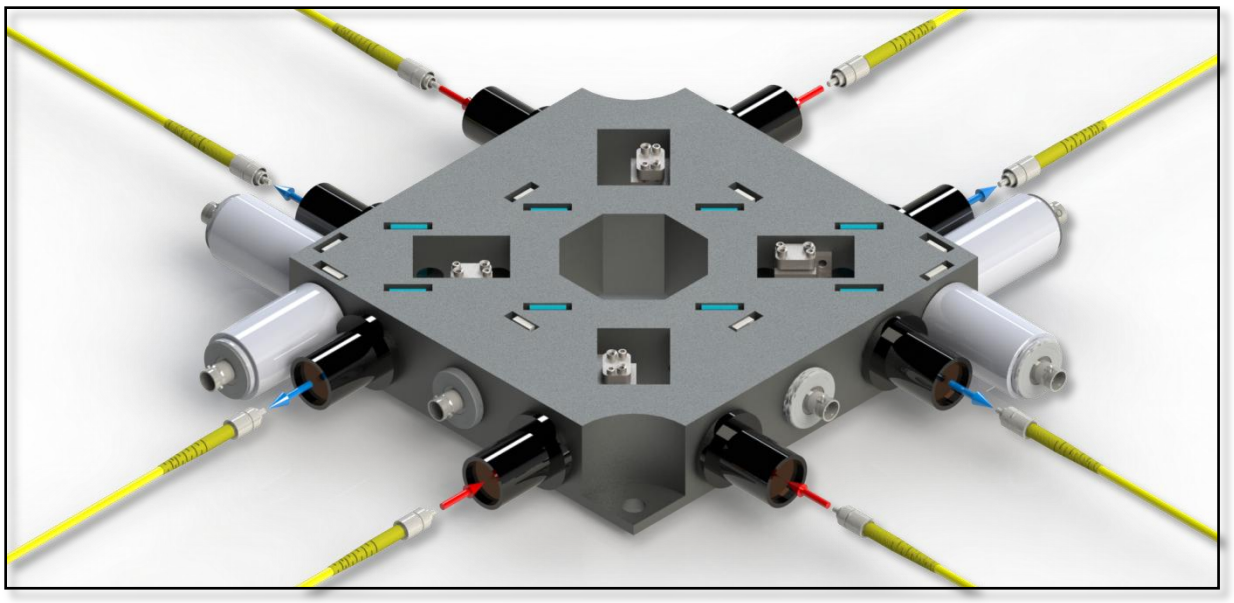

Figure C-8. An isometric depiction of a 4x4 optical switch.

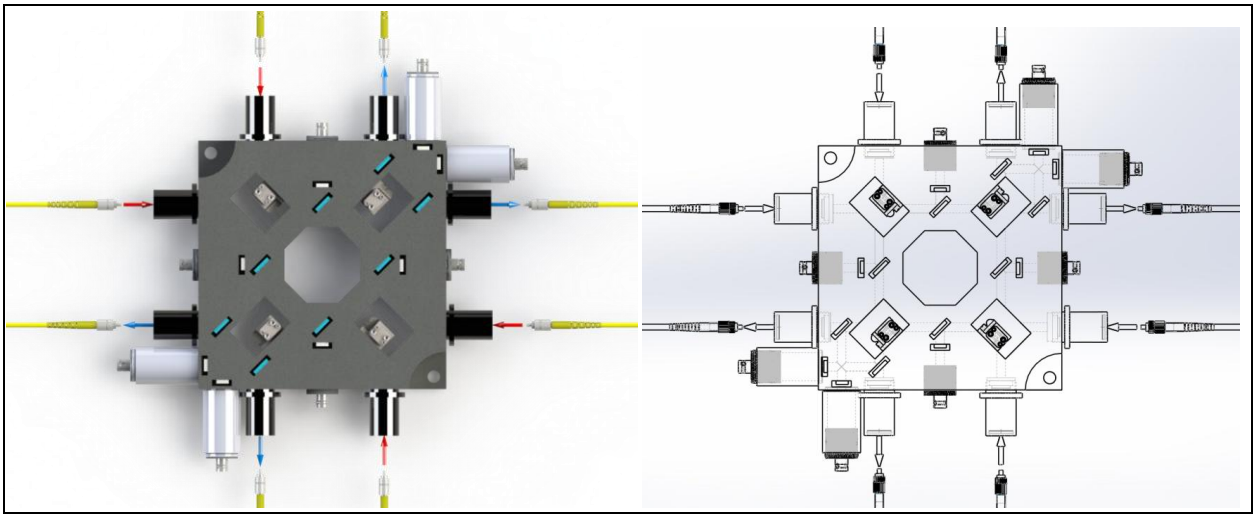

Figure C-9. (Left) The top realistic view of the 4x4 optical switch. (Right) The top view showing the hidden lines.

C-8. Final Thoughts

Participating in the Directed Energy Internship program at the ARL was beneficial in many ways. I was able to attain a working knowledge of *Dassault Systemes Solidworks*, *National Instruments LabWindows*, and *Corel Designer*. I also learned about SBS, CBC, and fiber-to-free-space collimation.

The most important aspect of this internship was experiencing being part of a research group and learning about the daily life of a scientist. Being engaged in research at the ARL allowed me to refine my ability to systematically approach a problem and consider all of the possible solutions. The office space is shared by several research groups, so I had the opportunity to attend seminars

and colloquiums, and see how scientists approach research problems on a daily basis. Tours of the Adelphi Laboratory Center and Aberdeen Proving Ground allowed me to see other Government labs and research projects in different areas.

C-9 References

1. Fan, T. Y. Laser Beam Combining for High-Power, High-Radiance Sources. *IEEE Journal of Selected Topics in Quantum Electronics* **2005**, *11* (3), 567–577.

2. Leger, J. R.; Holz, M.; Swanson, G. J.; Veldkamp, W. B. Coherent Laser Beam Addition: An Application of Binary-Optics Technology. *The Lincoln Laboratory Journal* **1988**, *1* (2), 225–246.

3. Vasilyev, A.; Petersen, E.; Satyan, N.; Rakuljic, G.; Yariv, A.; White, J. O. Coherent Power Combining of Chirped-Seed Erbium-Doped Fiber Amplifiers. *IEEE Photonics Technology Letters* **2013**, *25* (16), 1616–1618.

4. White, J. O.; Vasilyev, A.; Cahill, J. P.; Satyan, N.; Okusaga, O.; Rakuljic, G.; Mungan, C. E.; Yariv, A. Suppression of Stimulated Brillouin Scattering in Optical Fibers Using a Linearly Chirped Diode laser. *Optics Express* **2012**, *20* (14), 15872–15881.

NO. OF
COPIES ORGANIZATION

1 (PDF) DEFENSE TECHNICAL INFORMATION CTR
DTIC OCA

1 (PDF) DIRECTOR
US ARMY RESEARCH LAB
IMAL HRA

1 (PDF) DIRECTOR
US ARMY RESEARCH LAB
RDRL CIO LL

1 (PDF) GOVT PRINTG OFC
A MALHOTRA

1 (PDF) DIR USARL
RDRL SEE M
J WHITE

INTENTIONALLY LEFT BLANK.